Electronic Supplementary Material (ESI) for Nanoscale.

Supplementary Information

Rapid and sensitive fluorescence biosensor based on plasmonic PCR

Jingrui Wu,[†] Kunlun Jiang,[†] Hua Mi, Yuwei Qiu, Jiwoong Son, Hyun June Park, Jwa-Min Nam, Jung-Hoon Lee*

*Correspondence: junghlee@cityu.edu.hk

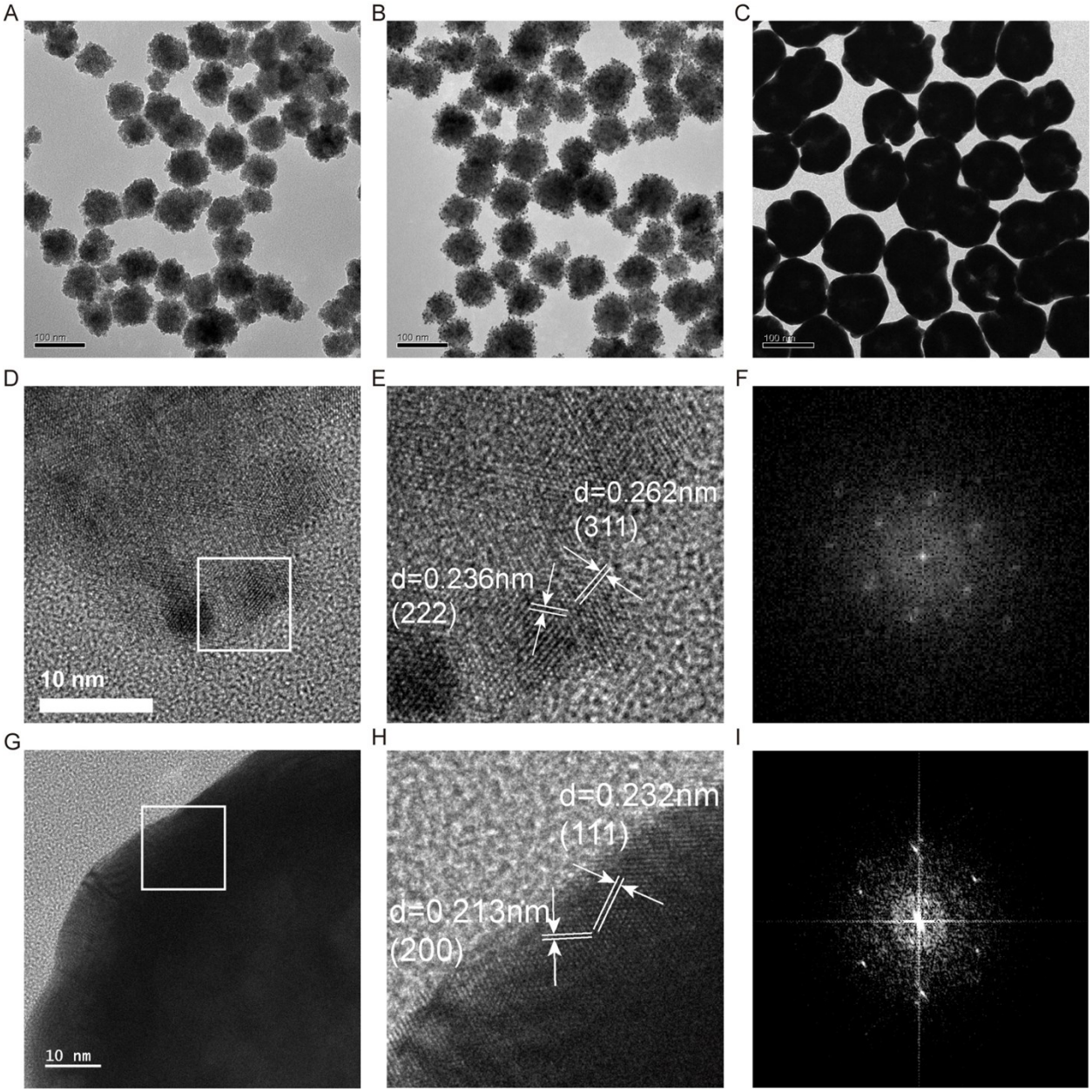

Figure S1. TEM images of (A) Iron oxide nanoclusters, (B) Au seed coated Iron oxide nanoclusters, (C) Au shell coated Iron oxide nanoclusters (Plasmonic magnetic nanoparticles, PMNs). HRTEM images and fast Fourier transform (FFT)

patterns of (D-F) iron oxide nanoclusters and (G-I) PMNs (E-F, and H-I are magnified images and FFT patterns show area in white box, respectively).

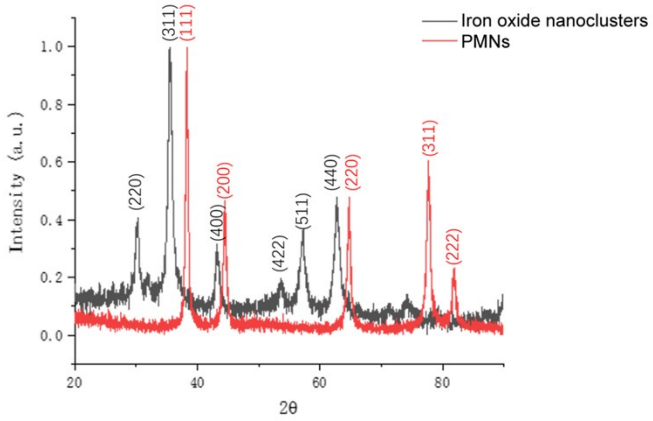

Figure S2. XRD patterns of iron oxide nanoclusters and PMNs.

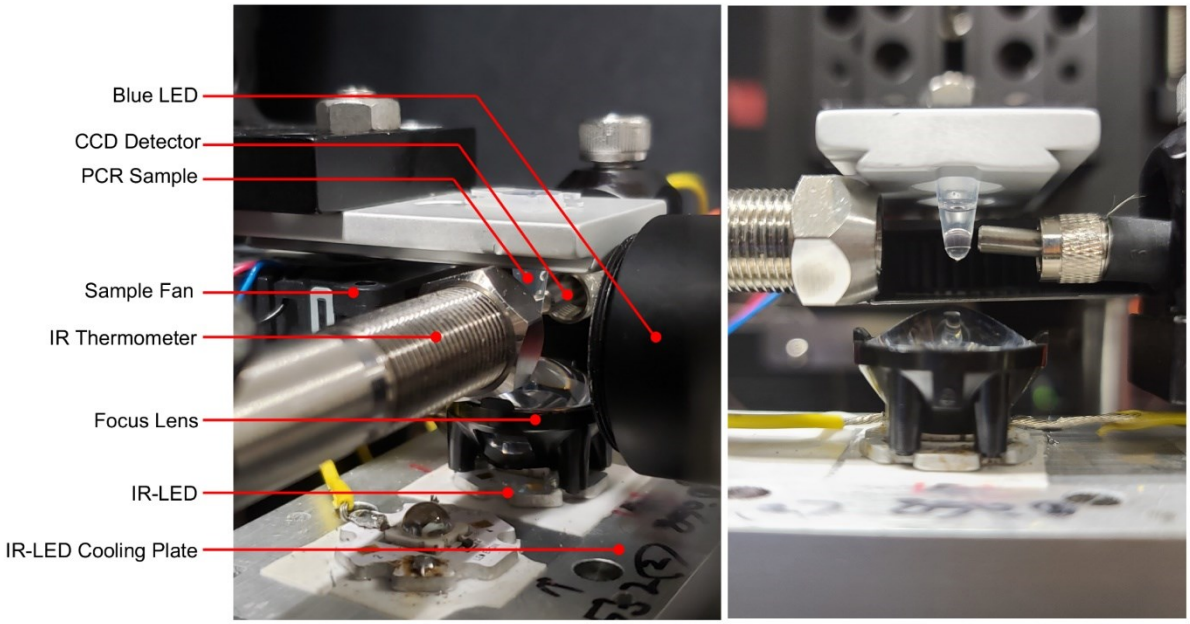

Figure S3. Photographs of home-build device for PPT-PCR.

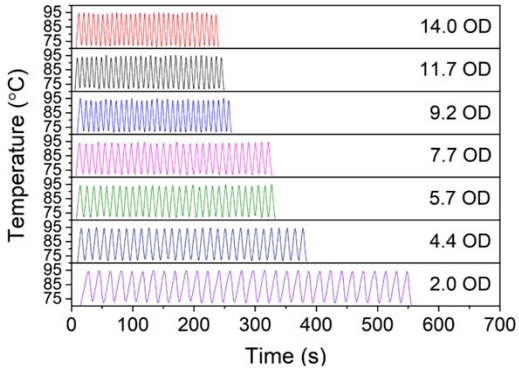

Figure S4. Temperature profiles for 30-thermocycles of solutions with different concentration of PMNs between 72 ˚C and 95 ˚C.

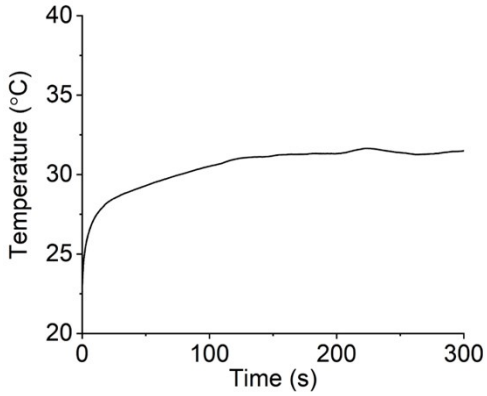

Figure S5. Temperature profile without PMNs under IR-LED irradiation.

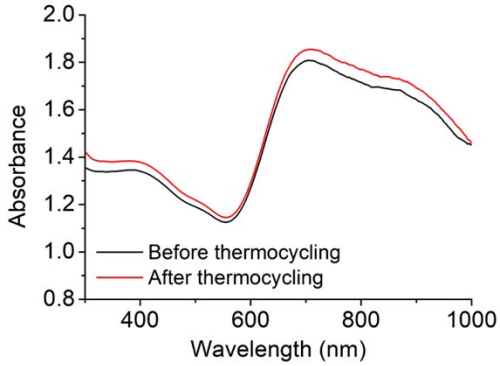

Figure S6. UV-Vis-IR spectrums of PMNs before and after thermocycling.

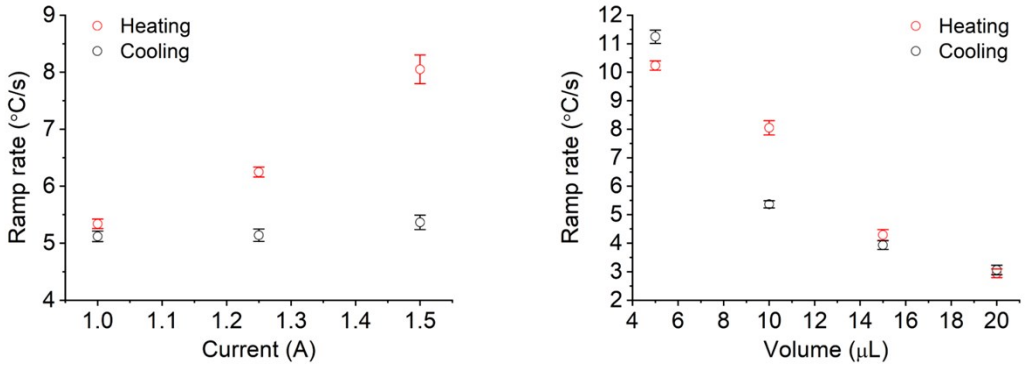

Figure S7. Optimization of working current (solution volume was fixed at 10 μL) and sample volume (working current was fixed at 1.5 A) for PPT-PCR. Concentration of PMNs was fixed at 14.0 OD.

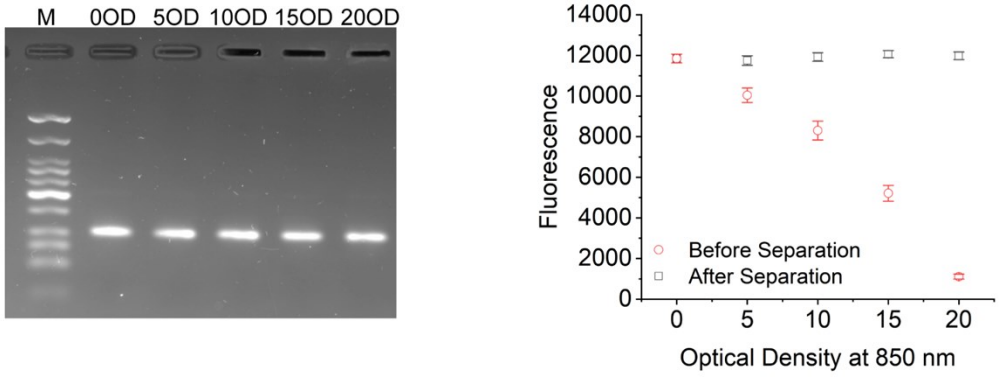

Figure S8. Left: Gel images from PPT-PCR amplifications with different concentration of PMNs. There was no significant suppression of high concentration nanoparticles for PCR amplification. There is no significant difference in the band intensity of PCR products amplified with different concentrations of PMN. This indicates that there is no significant inhibition of PCR amplification in the concentration range of the nanoparticles used in this study. Right: Study of fluorescence quenching effect by PMNs with different concentrations. To study the quenching effect of PMNs, end-point fluorescence intensity of PCR samples with different concentration of PMNs were measured before and after magnetic separation. Before magnet separation, fluorescence intensity getting lower while increasing the concentration of PMNs. However, after magnet separation, all the samples showed same fluorescence intensity. All the reactions in this figure were done with 10^6 copies/μL of Lambda DNA by conventional PCR instrument. The cycling condition was 95 °C, 20 seconds for initial denaturation; 95 °C, 5 seconds for denaturation; 72 °C, 10 seconds for annealing and extension, total 30 cycles.

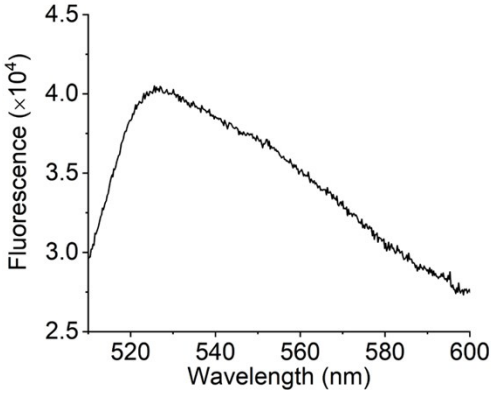

Figure S9. Characteristic fluorescence spectrum of DNA-SG after PPT-PCR and magnetic separation of PMNs.

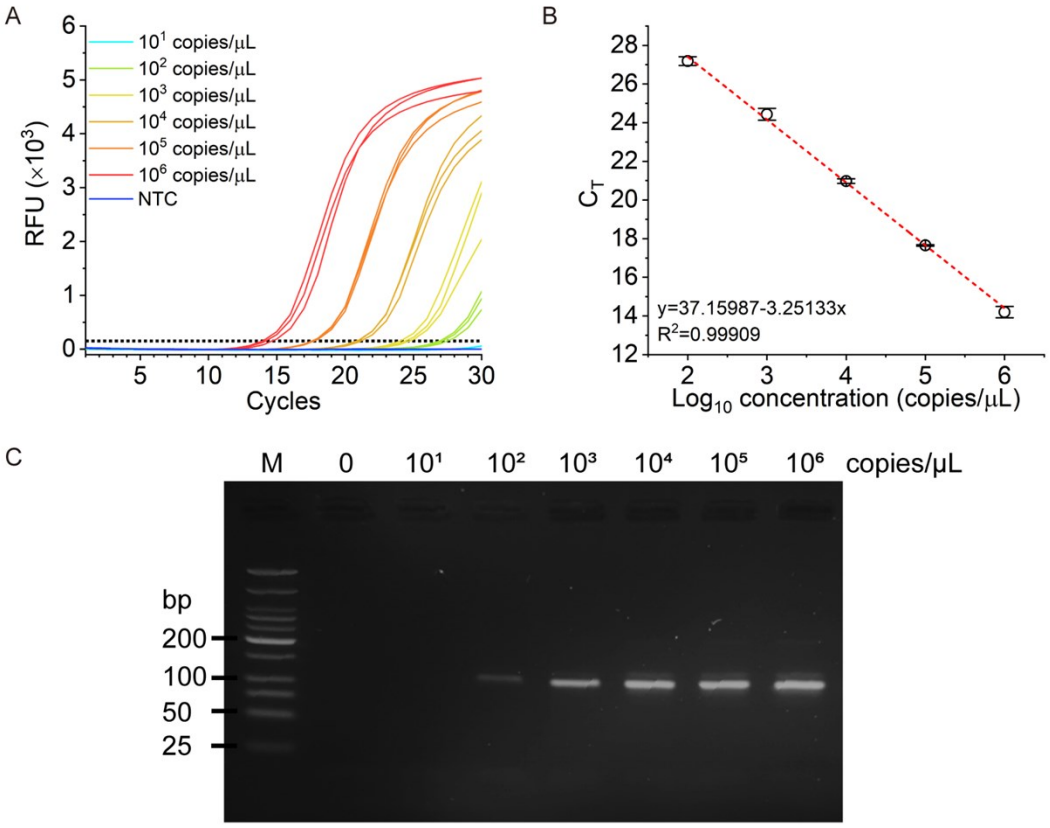

Figure S10. Results from conventional qPCR. (A) Real-time amplification curves of samples with different concentration of Lambda DNA template. (B) C_T values plotted against the Lambda DNA template concentrations. Error bars indicate standard deviation of triplicate measurements. (C) Gel electrophoresis image of samples after qPCR.

Calculation of the photothermal conversion efficiency

The photothermal conversion efficiency of PMNs was determined according to the previous method [1,2]. Detailed calculation was given as following:

$$\sum_i m_i C_i \frac{dT}{dt} = E_{abs} - E_{loss} \quad (1)$$

where E_{abs} is the heat induced by the absorption of the nanoparticles, which can be calculated by photothermal heating process. E_{loss} is the heat dissipated through the surrounding medium, which can be calculated by natural cooling process. t is the time, m_i and C_i are the mass and specific heat capacities of each element i comprising the entire physical system (i.e., PMNs, deionized water). The absorption and dissipation energy in Eq. (1) can be expressed as follows:

$$E_{abs} = P\left(1 - 10^{-A_\lambda}\right)\eta \quad (2)$$

$$E_{loss} = hS[T(t) - T_0] \quad (3)$$

where P denotes the incident 850 nm LED power employed to photoexcite the plasmon resonance of the PMNs, A_λ is the absorbance value of the PMNs at the 850 nm, η is the photothermal conversion efficiency. h is the heat transfer coefficient, S is the surface covered by the PMNs dispersion, and T_0 is the ambient temperature.

In our study, the mass of the actual PMNs was insignificant in comparison with the mass of the water (0.01 g). Moreover, the heat capacity of gold (0.129 $J \cdot g^{-1} \cdot K^{-1}$) is also much smaller than that of water (4.2 $J \cdot g^{-1} \cdot K^{-1}$). Thus, the mass and heat capacity of the entire PMNs dispersion can be assumed to be the one of deionized water (m_D=0.01 g, C_D=4.2 $J \cdot g^{-1} \cdot K^{-1}$). Then, Eq. (1) can be rewritten as follows:

$$\frac{dT}{dt} = \frac{P(1 - 10^{-A_\lambda})\eta}{m_D C_D} - \frac{hS[T(t) - T_0]}{m_D C_D} \quad (4)$$

When we only consider about the heating process in the thermal cycling, dT/dt (8.71 $^oC/s$) will be the average heating speed form 72 ^oC to 95 ^oC, T(t) is 95 ^oC, and T_0 is 25 ^oC, A_λ is 14.

$$\eta = \frac{\frac{dT}{dt} + \frac{hs[T(t) - T_0]}{m_D C_D}}{\frac{P(1 - 10^{-A_\lambda})}{m_D C_D}} \quad (5)$$

In Eq. (5), *P* and *hS* need to gain through additional experiments.

In order to get an accurate power density of LED light used only for photothermal conversion process, the spot size of the iris diaphragm was carefully adjusted to match with the size of the liquid solution (measured 3 mm in diameter) (Figure S11). The average measurement power of LED lights is 452 ± 21 mW (0.452 ± 0.021 J·s-1), which is the result of 5 measurements (Figure S11).

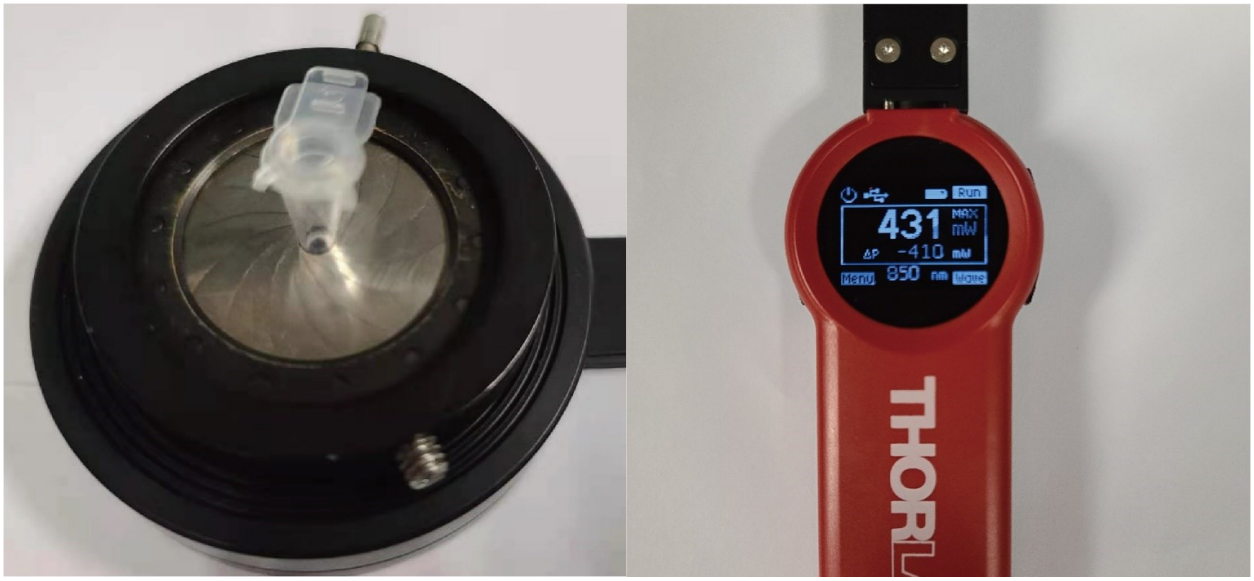

Figure S11. Measurement of power of light. Left: photograph of power meter with iris diaphragm (spot size is matched with the sample); Right: photograph of measured power of light.

In order to gain *hS*, we did an experiment with photothermal heating and natural colling processes. The aqueous solution of PMNs (14 OD) was under continuous irradiation of 850 nm LED until a temperature of 95 °C was reached. Subsequently, the LED was shut off, and the temperature decrease of the aqueous solution was recorded to measure the rate of heat transfer from the PMNs solution system to the environment (Figure S12A).

$$\theta = \frac{T_t - T_0}{T_{max} - T_0} \quad (6)$$

Where, T_t is the temperature at the time t, T_{max} is 95 °C, T_0 is 25 °C. Time constant for heat transfer from the system is determined to be τ_s=40.79 s by applying the linear time data from the cooling period (after 20 s) versus negative natural logarithm of driving force temperature, which is obtained from the cooling stage of Figure S12A (Figure S12B).

$$t = -\tau_s \ln(\theta) \quad (7)$$

$$hS = \frac{m_D C_D}{\tau_s} \qquad (8)$$

hS can be gained from Eq. (7) and Eq. (8).

Based on the experiment, photothermal conversion efficiency of the heating process of PMNs is η=96.8 %

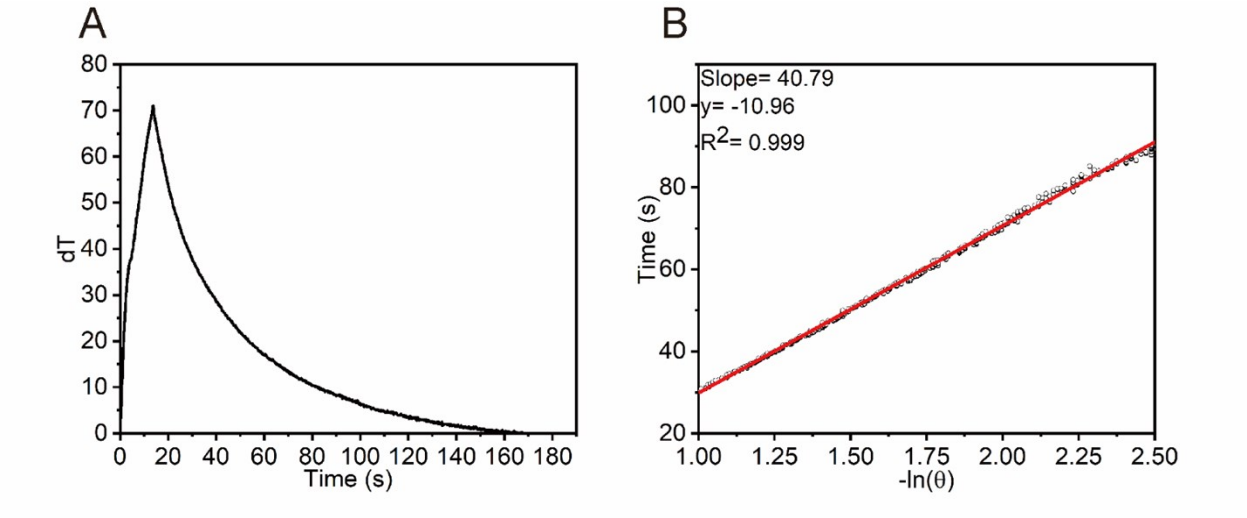

Figure S12. (A) Temperature changing of the PMNs in 10 µL solution upon 850 nm LED irradiation and then the LED was shut off. (B) Linear time data versus - ln θ obtained from the cooling stage of Figure S12A.

Table 1: Overview of different type of photothermal PCR.

Method	*Material*	*Target*	*Quantification method*	*PCR Amplification time (min)*	*Signal detection processing time*	*Detection range (copies/µL)*	*Limit of detection (copies/µL)*
Nano PCR [4]	MPNs (Core-shell $Zn_{0.4}Fe_{2.6}O_4$-Au)	SARS-CoV-2 (ss gRNA)	End-point fluorescence	6.5	3 min~12 min (50%~ 100% signal recovery)	None	3.2
PPT-qPCR[5]	AuBPs (Gold bipyramid nanoparticles)	M13mp18 (ds DNA)	Real-time fluorescence	5	Real-time	$7.3 \times 10^3 \sim 10^8$	7.3×10^3
Ultra-fast photonic PCR[6]	Au Film	Lambda DNA (ds DNA)	Gel electrophoresis	5	30 min	None	9.7×10^8
Our method	PMNs (Core-shell Fe_3O_4 nanocluster-Au)	Lambda DNA (ds DNA)	End-point fluorescence	5	15 s	$10 \sim 10^4$	3.3

References

1.Q. Tian, F. Jiang, R. Zou, Q. Liu, Z. Chen, M. Zhu, S. Yang, J. Wang, J. Wang and J. Hu, Acs Nano, 2011, 5, 9761-9771.

2. C. M. Hessel, V. P. Pattani, M. Rasch, M. G. Panthani, B. Koo, J. W. Tunnell and B. A. Korgel, Nano Lett., 2011, 11, 2560-2566.

3. Liu, X., Li, B., Fu, F., Xu, K., Zou, R., Wang, Q., ... & Hu, J. (2014). *Dalton transactions*, *43*(30), 11709-11715.

4. Cheong, J., Yu, H., Lee, C. Y., Lee, J. U., Choi, H. J., Lee, J. H., ... & Cheon, J. (2020). Fast detection of SARS-CoV-2 RNA via the integration of plasmonic thermocycling and fluorescence detection in a portable device. *Nature biomedical engineering*, 1-9.

5. Lee, J. H., Cheglakov, Z., Yi, J., Cronin, T. M., Gibson, K. J., Tian, B., & Weizmann, Y. (2017). Plasmonic photothermal gold bipyramid nanoreactors for ultrafast real-time bioassays. *Journal of the American Chemical Society*, *139*(24), 8054-8057.

6. Son, J. H., Cho, B., Hong, S., Lee, S. H., Hoxha, O., Haack, A. J., & Lee, L. P. (2015). Ultrafast photonic PCR. *Light: Science & Applications*, *4*(7), e280-e280.